

# Experimental verification of spectral grating interference in multiplexed volume holograms employed as broadband dispersive elements for solar concentrators

G.B. Ingersoll\*, D. Lin, and J.R. Leger

Dept. Of Electrical and Computer Engineering, Univ. of Minnesota, 200 Union St. SE,  
Minneapolis, MN, 55455

## ABSTRACT

Using diverse bandgap photovoltaic cells can improve solar conversion efficiency, but these systems also require efficient dispersive optics to direct portions of the solar spectrum onto the appropriate optimized cells. We use an extended coupled-mode model to show how multiplexed volume gratings interact with one another reducing efficiency in the diffraction orders of interest as well as increasing stray light under certain conditions. We conducted experiments with multiplexed gratings in dichromated gelatin to verify our theory. This technique reveals effects that cannot be seen through superposition of single grating models, which suggests that multiplexed gratings must be treated simultaneously when designing such a system.

**Keywords:** solar concentration, volume holography, multiplexed volume holograms, volume Bragg gratings, coupled-mode theory

## 1. INTRODUCTION

Split-spectrum photovoltaic (PV) cells have received a great deal of interest recently as an architecture for improving the efficiency of solar arrays [1]. One model for cell efficiency assumes that only photons with energy greater than the PV cell's band-gap will contribute useable energy to the system, and these photons will only contribute the band-gap energy. Based on this model, there are obvious advantages to heterogeneous solar arrays comprised of PV cells with different band-gap energies in which diffractive optical elements are employed to direct high-energy photons to high-band-gap cells (cf. Figure 1). Holographic spectrum splitters based on volume Bragg gratings have been proposed [2] for use in these heterogeneous systems.

Volume Bragg gratings and other volume holograms find many uses in laser and optical systems to focus, disperse, combine, and separate light. Multiplexed volume Bragg gratings (i.e. two or more Bragg gratings in the same holographic element) find uses in monochromatic systems (e.g. holographic data storage) and narrow-band systems such as wavelength-division (de)multiplexers for communications. Here we explore using a single holographic element in a broadband solar-spectrum splitting application to redirect a relatively wide subset of the incident spectrum into a new common angle where this energy can be more efficiently utilized. The element explored here employs multiplexed Bragg gratings to achieve a more ideally shaped spectral response. However, this work also explores the limitations in using multiplexed Bragg gratings in this manner and includes experimental demonstration of inter-grating interference effects which lead to loss of efficiency and stray light.

\* gbingersoll@gmail.com

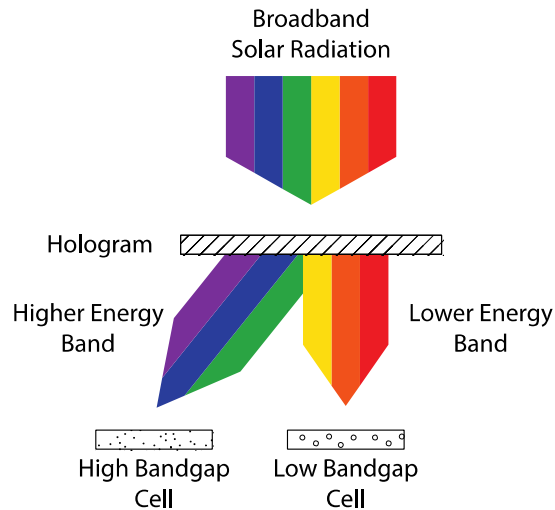


Figure 1: Holographic spectrum splitter (schematic). Solar radiation illuminates a single holographic element. The hologram directs a broad subset of the solar spectrum into a new, common direction where it falls on a high-band-gap PV cell optimized for the sub-band. The remaining lower energy portion of the spectrum passes through the hologram unaffected and falls on a PV cell with a lower band-gap energy.

## 2. THEORY

Given the goal of improving solar cell efficiency, and given a heterogeneous solar cell array, the remaining task is to design a diffractive structure to direct appropriate bands of the solar spectrum to the appropriate PV cells. The diffractive properties of volume Bragg gratings have been understood for some time [3], and these devices are valued for their theoretical high efficiency—as high as 100% for planar transmission-mode phase gratings—and single diffracted order.

A transmission-mode grating is represented in Figure 2 as a momentum diagram.  $\rho$  is the input wavevector giving the circle its radius  $2\pi n/\lambda$ , where  $n$  is the material index and  $\lambda$  is the vacuum wavelength of the incident light, and  $K$  is the grating vector—similar to a wavevector in that the grating vector denotes the frequency and tilt of a sinusoidal spatial variation in the index of refraction of the holographic material. The vector sum of the input wavevector and the grating vector then describes the wavevector,  $\sigma$ , of the diffracted order. If the input is Bragg-matched with the grating (in both angle and wavelength), the output vector will terminate on—or at least near—the momentum circle, and efficient power transfer into the output order can be expected.

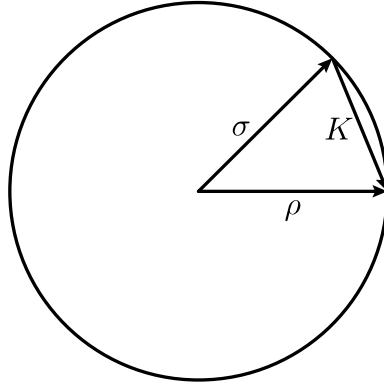


Figure 2: Basic momentum diagram of a single volume Bragg grating.  $\rho$  is the input wavevector,  $\sigma$  is the diffracted wavevector, and  $K$  is the grating vector. (By convention,  $\sigma = \rho - K$ .) In this example, the input is Bragg matched with the grating.

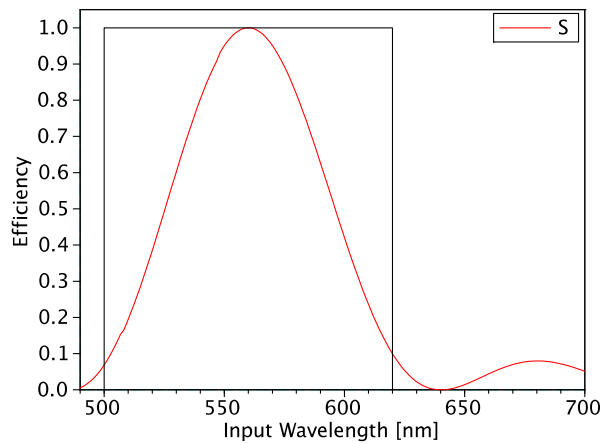


Figure 3: Diffraction efficiency of a single volume Bragg grating vs. input wavelength for a constant input angle. The black rectangle represents a hypothetical desired band-pass response. Note how the single grating's efficiency curve poorly approximates the desired band and also has non-zero efficiency outside the band.

The characteristic curve of the diffraction efficiency,  $S$ , of the grating's first order (corresponding to the wavevector  $\sigma$ ) versus input wavelength is shown in Figure 3 given a plane-wave input at a constant incident angle. Superimposed on the plot is a hypothetical and desired, but impractical diffraction efficiency curve for a split-spectrum solar application. Namely, this is a "brick-wall" band-pass filter diffracting all of the energy in a given band and leaving the other wavelengths unaffected. Note that the characteristic curve for a transmission mode volume Bragg grating is similar to a sinc function having a large central main lobe and many smaller side lobes. This shape is a poor approximation to the desired rectangular band-pass function as it provides high diffraction efficiency for only a small subset of the band of interest.

We aim to improve the band-pass response by adding a second grating to the diffractive element. The two multiplexed gratings have different central wavelengths but are constrained to have the same Bragg angles as depicted in the momentum diagram of Figure 4. The Bragg-angle constraint is not always required in multiplexed grating systems. Rather this constraint comes from the particular design of our spectral splitter and the chosen light collection and diffraction angles for the entire band of interest. Each grating is also dispersive (i.e. the diffraction angle of its first order varies with the wavelength of the input), however this effect is not considered further here.

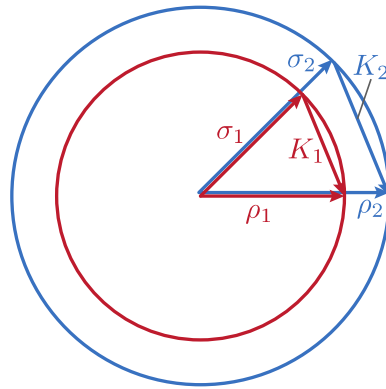


Figure 4: Momentum diagram illustrating the geometries of two multiplexed gratings for a spectrum splitting application. The Bragg angles defining the gratings are constrained to be identical, so their respective reference ( $\rho_i$ ) and first-diffraction-order ( $\sigma_i$ ) vectors are parallel. However, the gratings' central wavelengths differ (defined by the two circles' radii) resulting in a difference in the period of the gratings (i.e.  $K_1$  and  $K_2$  are parallel but have different lengths).

The superposition to two gratings is sketched in terms of diffraction efficiency over wavelength in Figure 5, illustrating an improvement in the overall efficiency of the system. However, this representation is clearly non-physical as the sum of the efficiencies of the two diffraction orders exceeds 100% in certain cases. That is, this simple model (i.e. superposition of the results for each grating of Kogelnik's single-grating model) leads to a violation of conservation of energy. The resolution to this paradox has been previously explored for monochromatic systems [4] and narrow-band WDM waveguide systems [5]. Similar issues arise in broadband multiplexed-grating systems that require similar input and output angles for the gratings.

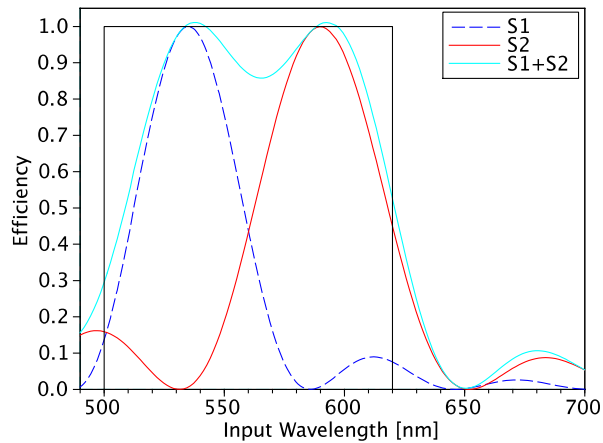


Figure 5: Diffraction efficiency of a two volume Bragg gratings vs. input wavelength for a constant input angle. The black rectangle represents a hypothetical desired band-pass response. The efficiencies,  $S_1$  and  $S_2$ , of the two diffracted orders (corresponding to the  $\sigma_1$  and  $\sigma_2$  wavevectors respectively) are plotted along with the sum of these two curves. Note how this reveals a shortcoming in the model because the combined efficiency exceeds 100% in two regions.

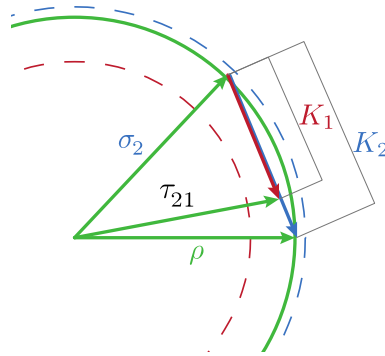


Figure 6: Momentum diagram of the multiplexed grating pair excited by a wavelength slightly higher than the central wavelength of Grating 2. The dashed circles correspond to the circles in Figure 4.

The resolution to the violation of conservation of energy described above comes from noting that the addition of a second grating gives rise to cross-coupled orders. That is, light diffracted by one grating is subsequently diffracted by the other before it exits the hologram. This results in reduced efficiency in the diffractive order of interest and also introduces stray light into the system. This effect is illustrated in the momentum diagram of Figure 6. Because the vector combination of the incident wave-vector and both grating vectors (i.e.  $\tau_{21} = \rho - K_2 + K_1$ ) lies near the momentum circle representing the operating wavelength, we qualitatively expect some non-zero output power in the direction given by the new wavevector,  $\tau_{21}$ .

The precise impact of this cross-coupling phenomenon cannot be determined by the momentum diagram. Instead it must be calculated by extending the coupled-wave model of Kogelnik to include more simultaneous diffraction orders. Extensions to Kogelnik's model have been previously explored for monochromatic and narrow-band systems. The model used here is extended further to include an arbitrary number of cross-coupling—this becomes particularly important for systems with more than two gratings—and also to include the possibility of +1 as well as -1 diffraction orders (e.g.  $\sigma_{+1} = \rho + K_1$ ). This latter point is important in broadband systems. Broad efficiency curves (as a function of wavelength) can be achieved with long-period gratings (i.e. short grating vectors). In the context of a momentum diagram, note that if the input is nearly Bragg-matched with the -1 order of a grating,  $K$ , with a long period (short vector), in many geometrical cases, the input will also be nearly Bragg-matched with the grating's +1 order.

Figure 7 shows the basic effect of cross-coupling between the two gratings in the theoretical holographic element discussed so far consisting of two gratings constructed with identical Bragg angles but differing central wavelengths. In addition to reducing power in the desired output orders ( $\sigma_1$  and  $\sigma_2$ ), additional output orders ( $\tau_{12}$  and  $\tau_{21}$  with efficiencies  $T_{12}$  and  $T_{21}$  respectively) arise producing stray light in the system.

A key point here is that the cross-coupling phenomenon's impact cannot be calculated by superposition of the results of individual single-grating calculations. Note in comparing Figure 5 and Figure 7 that some zeros for the single grating case become non-zero when the gratings are multiplexed. Also, obviously, single grating calculations do not predict cross-coupled orders at all.

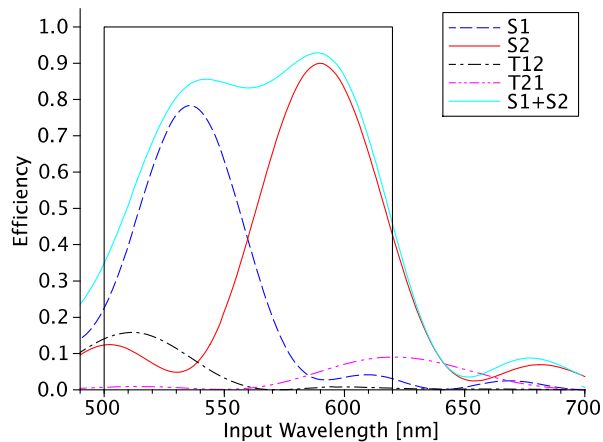


Figure 7: Diffraction efficiency of two multiplexed volume Bragg gratings vs. input wavelength for a constant input angle calculated from the extended model. The black rectangle represents a hypothetical desired band-pass response. The efficiencies,  $S_1$  and  $S_2$ , of the two gratings' first diffracted orders (corresponding to the  $\sigma_1$  and  $\sigma_2$  wavevectors respectively) are plotted as well as the sum of these two curves. This is the useful light in the solar spectrum splitting system as these orders are designed to have a nearly common output angle over the band of interest. Also plotted are the efficiencies of two cross-coupled orders,  $\tau_{12}$  and  $\tau_{21}$  with efficiencies  $T_{12}$  and  $T_{21}$  respectively, which indicate stray light in the system.

### 3. EXPERIMENT

#### 3.1 Method

To demonstrate these effects in a multiplexed-grating holographic element, we constructed such elements in our lab using PFG-04 dichromated gelatin plates and characterized their performance at multiple wavelengths. The recording setup used a Coherent Verdi laser operating at 532nm and up to 5W. This beam was split, and each half was expanded and redirected to the target plate by a mirror mounted on a rotation stage. In this manner, the exposure at the target was a close approximation of two interfering plane waves, and the incident angles of the recording beams could be easily adjusted to expose gratings with the prescribed period and tilt.

Some previous work has been published utilizing this particular material [6], and we performed some further experimentation to determine a valid operating point for our demonstration elements. The predicted cross-coupling effects are most pronounced from gratings with high diffraction efficiency, where a practical wavelength splitting element would be designed. However, limitations due to the recording medium forced us to scale back this efficiency. The initial system goal was to multiplex two relatively broadband gratings centered at 532nm and 632nm. The bands were arbitrarily chosen such that the peak diffraction wavelength of one grating would roughly correspond with a zero in the diffraction efficiency curve of the other grating. Given these constraints, for high efficiency, the necessary index modulation values for the gratings (given an emulsion thickness of roughly 30 microns) combined to exceed the available dynamic range of the material. Exceeding the dynamic range of the material would result in distortion of the nominally sinusoidal phase gratings of the mathematical model which, in turn, would lead to depressed diffraction efficiency and possibly higher-order effects. To avoid this, exposure energies were kept relatively low which led to reduced peak diffraction efficiencies. However, the efficiency is sufficiently high to enable accurate measurements of the cross-coupling phenomenon in the experimental data.

An additional drawback to generating low-to-medium efficiency transmission gratings in this material is the high variability of diffraction efficiency as a function of exposure energy. Because the efficiency vs. exposure curve is quite steep in our operating regime, minor variations in average recording beam power, emulsion thickness, and chemical parameters during development result in variations in the peak diffraction efficiency of the resulting gratings. To control for these variations, exposures of both single and multiplexed gratings were arranged on a single dichromated gelatin

plate. The two multiplexed gratings of a given experimental pair only partially overlap on the plate allowing characterization of each grating individually as well as characterization of the multiplexed pair.

Diffraction efficiency of a set of gratings is dependent on Bragg-matching in angle and wavelength simultaneously, and a grating's Bragg angles depend on the wavelength of the incident light. The mathematical model used here accommodates simultaneous detuning in both angle and wavelength, so measuring experimental diffraction efficiency as a function of incident angle allows for a less-complicated laboratory setup for grating characterization: the present setup only requires a rotation stage rather than a tunable source.

First, each grating's diffraction efficiency is measured with a 632nm source as a function of incident angle around one of the grating's Bragg angles. This data along with a measurement of the other Bragg angle is fed back into the model, and the modulation depth of the grating is adjusted in the model to achieve a good fit to the experimental data. Matching the model to experimental data in this manner accounts for positioning error during recording and variations in thickness and grating period as a result of processing (i.e. gelatin swelling). After this is performed for each grating individually, the gratings are modeled together and compared with measurements of the multiplexed gratings in the gelatin plate. Finally, the multiplexed pair is measured again versus input angle but with a 532nm source. This is shown to match the model as well suggesting efficacy of the model over angular and wavelength variations despite not measuring the gratings over a continuum of wavelengths.

### 3.2 Results

The two gratings of a pair were measured individually with an expanded, collimated beam from a 632nm He-Ne laser source. The modeled diffraction efficiency of Grating 1's  $\sigma$  order (non-multiplexed) vs. input angle is plotted along with experimental data in Figure 8 for 632nm illumination. This experimental data drove the model to determine the grating characteristics shown in Table 1. A similar procedure determined the characteristics for Grating 2. We note that we were easily able to make single transmission gratings with greater than 90% diffraction efficiency with this material, and emphasize that the reduced efficiency was specifically chosen to eliminate possible nonlinear effects that would compromise the measurements taken from the superposition.

Table 1: Grating properties determined by matching the mathematical model to experimental measurements for non-multiplexed gratings. (Note that while thickness data here is determined through matching efficiency curves, this thickness is corroborated by profilometer measurements in our lab suggesting a range of 28–33 microns depending on material age, developing conditions, etc.)

	<b>Grating 1</b>	<b>Grating 2</b>
<b>Bragg Angle 1 [deg., air at 632nm]</b>	22.00	18.92
<b>Bragg Angle 2 [deg., air at 632nm]</b>	-31.17	-31.17
<b>Period [micron]</b>	0.71	0.75
<b>Modulation</b>	0.004	0.004
<b>Thickness [micron]</b>	29	29

Figure 9 and Figure 10 then show the diffraction efficiencies of the various output orders of the multiplexed grating pair vs. input angle for 632nm and 532nm illumination respectively. In these figures, the theoretical efficiency curves of the individual gratings are included for reference. Note not only the decrease in peak efficiency for each grating but also the corresponding increase in power in the two cross-coupled orders (curves  $T_{12}$  and  $T_{21}$ ).

Some discrepancy between the theoretical and experimental data can be explained because the individual and multiplexed gratings were measured at different locations on the holographic plate. Although we tried to keep these variations to a minimum, spatial variation in beam power and/or local variations in plate thickness undoubtedly caused localized variation in grating modulation.

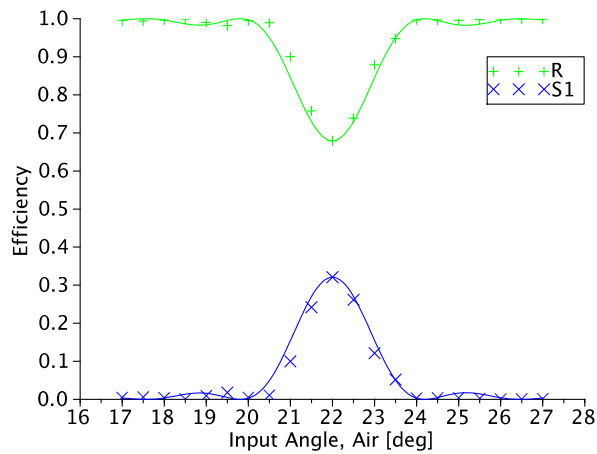


Figure 8: Experimental efficiency measurements of Grating 1 (not multiplexed) as a function of input angle with a 632nm source. Here  $S_1$  is the efficiency of Grating 1's first ( $\sigma$ ) diffraction order, and R is the "efficiency" of the grating's zero order (i.e. the undiffracted portion of the reference beam exiting the hologram). The theoretical model's parameters were adjusted to generate the solid curves.

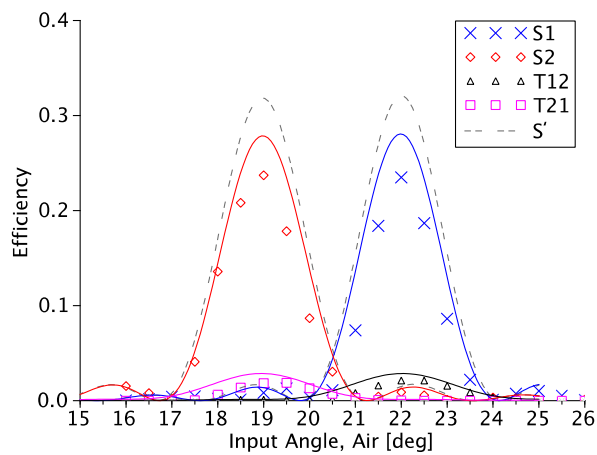


Figure 9: Experimental efficiency measurements of the multiplexed grating pair as a function of input angle with a 632nm source. The zero order efficiency (R) is not shown for clarity. Dashed curves denoted  $S'$  indicate expected S-order efficiency for each grating when not multiplexed.

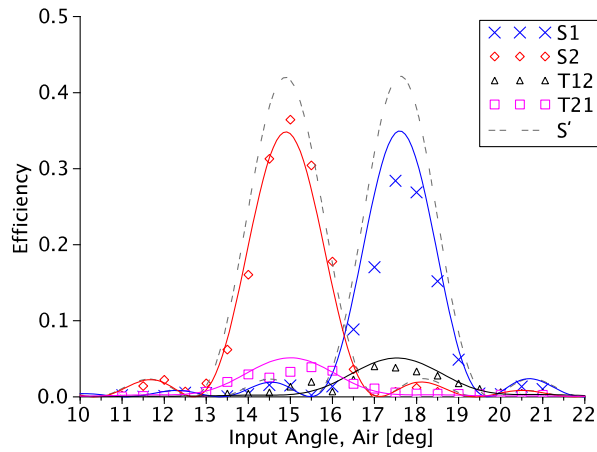


Figure 10: Experimental efficiency measurements of the multiplexed grating pair as a function of input angle with a 532nm source. The zero order efficiency (R) is not shown for clarity. Dashed curves denoted S' indicate expected S-order efficiency for each grating when not multiplexed.

To predict the performance of this multiplexed system over a given wavelength band, these gratings' modeled efficiency curves as a function of wavelength at a fixed incident angle of 18.5 degrees is plotted in Figure 11. Experimental data is superimposed at the two wavelengths measured suggesting a good match with the overall model.

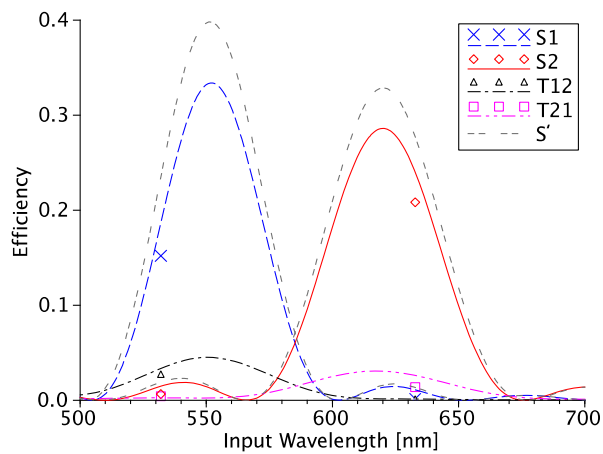


Figure 11: Experimental gratings' efficiency modeled as a function of input wavelength at an incident angle of 18.5 degrees (in air). Dashed curves denoted S' indicate expected S-order efficiency for each grating when not multiplexed. Symbols indicate experimental data measured at the given incident angle using 532nm and 632nm laser sources. The zero order (R) is not shown for clarity.

To demonstrate that the results here are not due to non-linear effects in the material, a separate experiment was conducted with slightly different grating characteristics (see Table 2). Here Grating 1 is unchanged from the previous data, but Grating 2's construction angles were modified slightly to change its second Bragg angle. With this new geometry, essentially no inter-grating interference and no cross-coupled power is expected from the modeled system. The plot in Figure 12 shows modeled and measured diffraction efficiency versus input angle at 632nm. As the model predicts for this geometry, the cross-coupled orders are completely absent. This is true even considering that the modulation for these gratings was slightly stronger than for the case of interfering gratings.

Table 2: Non-interfering grating properties determined by matching the mathematical model to experimental measurements for non-multiplexed gratings.

	Grating 1	Grating 2
<b>Bragg Angle 1 [deg., air at 632nm]</b>	22.00	18.92
<b>Bragg Angle 2 [deg., air at 632nm]</b>	-31.17	-39.50
<b>Period [micron]</b>	0.71	0.66
<b>Modulation</b>	0.0045	0.0045 </td
<b>Thickness [micron]</b>	29	29

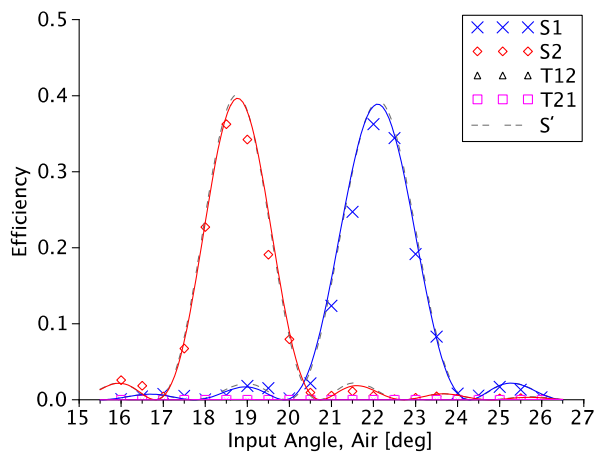


Figure 12: Modified geometry gratings' efficiency as a function of input angle with a 632nm laser source. Note that power is absent from cross-coupled orders (curves  $T_{12}$  and  $T_{21}$ ). Dashed curves denoted  $S'$ —essentially coincident with the solid curves—indicate expected S-order efficiency for each grating when not multiplexed.

#### 4. DIRECTIONS FOR FUTURE WORK

This work experimentally corroborates previous research applying multiplexed volume gratings to multi-wavelength systems. In addition, this work reinforces the need to have an extended model of these systems to ensure that all diffractive orders of interest are considered when modeling broadband multi-wavelength multiplexed systems.

This extended mathematical model is of particular importance to the types of systems discussed here. When multiplexed grating pairs are applied to spectral-splitting in this way, the gratings' Bragg angles are constrained to be identical. Further, their central wavelengths must be defined to be relatively close together to avoid gaps in the diffracted spectrum. Often cited rules-of-thumb from e.g. WDM systems—such as separating channels by many times the channel bandwidth to avoid crosstalk—cannot be applied in this regime. However, if design decisions regarding operating angles and central wavelength separation are not considered together (i.e. if the gratings are not modeled as a complete coupled system), diminished performance will result.

Future work will tailor this spectral-splitting architecture to a more practical case, improve overall system efficiency in practice, and fully characterize the system as a function of operating wavelength.

#### REFERENCES

- [1] Barnett, A., Kirkpatrick, D., et. al., "Very high efficiency solar cell modules," *Prog. Photovolt: Res. Appl.* 17(1), 75-83 (2009).
- [2] Lin, D., Torrey, E., Leger, J., and Cohen, P., "Lossless holographic spectrum splitter in lateral photovoltaic devices," *IEEE Photovoltaic Specialists Conference*, 000894-000898 (2011).
- [3] Kogelnik, H., "Coupled Wave Theory for Thick Hologram Gratings," *Bell Syst. Tech. J.* 48(9), 2909-2947 (1969).
- [4] Alferness, R. and Case, S. K., "Coupling in Doubly Exposed, Thick Holographic Gratings," *J. Opt. Soc. Am.* 65(6), 730-739 (1975).
- [5] Minier, V. and Xu, J. M., "Coupled-mode Analysis of Superimposed Phase Grating Guided-wave Structures and Intergrating Coupling Effects," *Opt. Eng.* 32(9), 2054-2063 (1993).
- [6] Villamarin, A., Atencia, J., Collados, M. V., and Quintanilla, M., "Characterization of transmission volume holographic gratings recorded in Slavich PFG04 dichromated gelatin plates," *Applied Optics* 48(22), 4348-4353 (2009).